Contents lists available at ScienceDirect

Arabian Journal of Chemistry

journal homepage: www.ksu.edu.sa

Synthesis of lignin-based covalent organic frameworks bio-composites: Quantitative evaluation of adsorption-photoreduction of hexavalent chromium

Huiying Hu, Kaijian Bi, Haizhong Yu, Pengjiao Tian *, Xiqing Wang *

College of Food Technology and Chemical Engineering, Hubei University of Arts and Science, Xiangyang, Hubei Province, China

ARTICLE INFO

Keywords:
Lignin
Covalent organic frameworks
Heavy metals
Photocatalytic
Reactive oxygen species

ABSTRACT

A novel bio-covalent organic framework (COF: TpPa-SO_3H/Lignin) based on TpPa-SO_3H and lignin from lignocellulose was synthesized for chromium (Cr(VI)) remediation in this study. Results showed that TpPa-SO_3H/Lignin had a highest adsorption capacity at the range of 5 ~ 75 mg/L Cr(VI) under 10 mg/L dosage, in which 100 % Cr(VI) could be removal within 120 min. Likewise, the introduction of lignin improved the visible light response range, charge separation and photogenerated carriers, thereby improving the photocatalytic efficiency of Cr(VI) by TpPa-SO_3H/Lignin. The highest photocatalytic efficiency of TpPa-SO_3H/Lignin (98.56 %) was observed at the acidic conditions. ESR result shows that e- and $\cdot O_2^-$ are generated and played an important role during the photocatalytic reaction, while the contribution of ·OH to Cr(VI) photoreduction is negligible. This study presents a sustainable and efficient approach to mitigating Cr(VI) pollution. It opens up avenues for further exploration of lignocellulose-derived materials in environmental applications and highlights the potential of COFs in addressing heavy metal contaminants.

1. Introduction

Chromium (Cr), a significant environmental contaminant, arises from various industrial activities such as electroplating, tanning, and textile dyeing, presenting substantial health and ecological risks (Izzudin et al., 2021; Malaviya and Singh, 2011). The Ecological Environment Status Bulletin of China identifies heavy metals, particularly Cr, as the primary contributors to soil pollution (Ministry of Environmental Protection and the Ministry of Land and Resources, 2014). Environmentally, Cr exists mainly in two forms: Cr(III) and the more toxic Cr(VI) (Su et al., 2016). Cr(VI), in particular, is recognized for its high solubility and mobility in water, allowing it to easily permeate through soil layers and contaminate groundwater sources (Deng et al., 2023). It is highly toxic to living organisms, causing severe health issues such as cancer, kidney damage, and liver failure in humans, and posing significant risks to aquatic ecosystems (Ma et al., 2024). The high oxidative state of Cr (VI) enables it to penetrate cellular membranes more efficiently than Cr (III), leading to greater bioavailability and toxicity. Traditional remediation methods primarily address Cr(III) complexities, leading to less effective Cr(VI) treatments (Prasad et al., 2021; Nakkeeran et al., 2018; Jiang et al., 2019). Therefore, it is crucial to develop and implement eco-friendly and sustainable strategies for Cr(VI) remediation to ensure soil health.

Various techniques have been applied to remediate the pollutant water, comprising the chemical catalysis (Liu et al., 2023a), physical adsorption (Fan et al., 2021), photodegradation (Shen et al., 2022) and biodegradation (Jiang et al., 2022). For instance, physical adsorption techniques, using materials like activated carbon or nanoparticles, effectively remove low concentrations of Cr (VI) but generate secondary waste and require regeneration of the adsorbent materials (Fan et al., 2021). Photodegradation, employing particulate materials, has emerged as a cost-effective and efficient strategy for Cr(VI) remediation (Zhong et al., 2023; Sun et al., 2023; Wang et al., 2024a). Currently, various materials such as porous organic polymers (Cao et al., 2022; Li et al., 2023a), metal organic frameworks (MOFs) (Sun et al., 2023), active carbon (Liu et al., 2023b), and covalent organic frameworks (COFs) (Zhong et al., 2023; Chen et al., 2023; Ma et al., 2024) have been harnessed for this photodegradation process. COFs, innovative porous crystalline materials, composed of organic building blocks connected via covalent bonds, provide well-defined, ordered structures that can be fine-tuned at the molecular level (Côté et al., 2005). These frameworks are distinguished by their high surface areas and porosities, rendering

* Corresponding authors.
E-mail addresses: 13120018505@163.com (P. Tian), Xiqingwang91@163.com (X. Wang).

https://doi.org/10.1016/j.arabjc.2024.105980
Received 8 May 2024; Accepted 21 August 2024
Available online 23 August 2024

them suitable for diverse applications including gas storage, separation, catalysis, and in electronic devices (Zeng et al., 2016; Li et al., 2022c; Yin et al., 2021). Previous research indicated that COFs, offering high specific surface areas, uniform pore sizes, and robust chemical stability, effectively adsorb various pollutants like PFAS, U(VI) and Pb^{2+} (Zhong et al., 2023). Moreover, the extended π-π conjugated structures within COFs augment their potential as photocatalysts. For instance, Li et al. (2022) demonstrated a method to photodeposit platinum clusters in situ on a COF, culminating in a substantial enhancement of the photocatalytic hydrogen evolution rate of 424.32 $\mu mol\ g^{-1}\ h^{-1}$ at 1 wt% platinum loading (Li et al., 2022a). Despite these merits, the application of COFs in the photodegradation of pollutants remains limited, primarily attributed to the low charge transfer efficiency between monomers, which attenuates their photocatalytic activity (Zhang et al., 2022; Zhong et al., 2023).

One intriguing method to augment photocatalytic performance is via modification of the conjugated structure within COFs to optimize light absorption. However, it is important to recognize that this strategy may negatively impact the porosity of the COFs (Peng et al., 2021; Yang et al., 2022a). In response, substantial efforts have been directed towards incorporating electron transfer groups into the COFs structure to enhance electron separation and conversion (Sheng et al., 2019; Yang et al., 2022b). For instance, the recent work by Shan et al. (2023) featured 2D porphyrin-based donor–acceptor (D-A) COFs, leading to a remarkable reshaping of their morphology and structure, facilitating efficient charge transfer and separation of photogenerated electron-hole pairs. This innovative approach resulted in the highly selective oxidation of sulfides (97 % conversion, 99 % selectivity) and reductive dehalogenation of 2-bromoacetophenone (99 % conversion, 82 % yield) (Shan et al., 2023). Nonetheless, the substantial costs and extensive usage of organic solvents in these reactions pose considerable challenges to their commercialization and industrial application. Thus, there exists an urgent need to develop high-performance COFs utilizing affordable, eco-friendly materials. Harnessing natural products or waste for COF synthesis offers a viable solution. Lignin, a by-product of the pulping industry, is enriched with complex polyphenols such as catechol and pyrogallol, presenting properties favorable for covalent or physical interactions with assorted compounds. This renders lignin as a promising candidate to construct supramolecular complexes beyond its conventional function as a fuel source. Moreover, the quinone structure in lignin functions as an electron transfer carrier to facilitate electron transfer and the catalytic reduction of O_2 to generate reactive oxygen species (Xie et al., 2023). Nevertheless, the structural and functional aspects of lignin-based COFs, particularly in Cr(VI) remediation, still require further comprehensive exploration.

Therefore, this study aims to synthesize and characterize lignin-based COFs and evaluate their effectiveness in the adsorption-photoreduction of Cr(VI), contributing to the development of sustainable and efficient remediation strategies. First, the lignin formed derived from corn stover combined with COFs was firstly prepared and synthesis for the bio-composites in this study. Then, the structure of bio-composites was determined via the UV–vis DRS spectra, PL spectra, ESR, FTIR and XPS. Finally, the remediation effectiveness of bio-composites was investigated via the adsorption and photodegradation experiments.

2. Materials and methods

2.1. Materials

Corn stover, obtained from the Xiangyang City, Hubei Province, China, was used in this study. Chemicals including sodium hydroxide (NaOH), urea, N, N-dimethylacetaminde (DMAc), 2,5-diaminobenzenesulfonic acid (Pa-SO_3P), p-toluenesulfonicacid (PTSA), acetic acid, 2,4,6-triformylphloroglucinol (Tp), and acetone were purchased from Macklin Co. Ltd. (China).

2.2. Separation of the lignin from corn stover

The extraction of lignin from corn stover followed a procedure described in the previous study (Chen et al., 2021). Briefly, 10 g corn stover was first mixed with 100 mL of NaOH/urea solution (2:3 w:w ratio) and agitated for 90 min at 60 ℃ and 150 rpm. Following liquid–solid separation, the resulting suspension was acidified with HCl to a pH of 1 and left overnight. This mixture was then centrifugally filtered to yield a black lignin precipitate.

2.3. Preparation the bio-composite

The COFs powders preparation method was meticulously formulated according to the previous research (Liu et al., 2023c). Briefly, 170 mg of Pa-SO_3H and 860 mg of PTSA were first ground together in a mortar for 10 min. Subsequently, 150 mg of Tp was added, and the grinding continued for 30 min. Water was then carefully added to the mixture, which was further processes for 5 min before drying in a vacuum oven at 120 ℃ for 10 min. The resultant red powder was cleansed with water, DMAc, and acetone, and finally dried under vacuum at 70°C for 12 h, culminating in the COF materials. The bio-material synthesis was preformed as per the follow steps. Initially, 0.2 g of COF material was dispersed in 100 mL of saturated lignin solution using sonication for 30 min. Then, 74.5 mg of Tp was added, and the mixture was left to rest overnight. The final step involved drying the mixture under vacuum at 70°C for 24 h to procure the bio-composite (Fig. 1).

2.4. Characteristics of the bio-composites

The characteristics of functional groups and element compositions of bio-composites materials were determined by the Fourier Transform Infrared (FT-IR) spectra (Varian Excalibur 3100, USA) and X-ray photoelectron spectroscopy (XPS, Thermoescalab 250Xi, USA). The evolution of crystalline structure of the bio-COFs were determined using the X-ray Diffraction (XRD) spectra (D8-Advance, Bruker, Japan). The specific surface area was quantified using the Brunauer-Emmett-Teller (BET) method under N_2 condition. The electrochemical properties of TpPa-SO_3H and TpPa-SO_3H/lignin was determined by utilizing the Ultraviolet–visible Diffuse Reflectance Spectra (UV–vis DRS, Shimadzu UV-2600 spectrophotometer), Photoluminescence (PL) spectra (HORIBA FluoroMax spectrophotometer) and Electrochemical impedance spectra (EIS, Shanghai Chenhua CHI 660E workstation). Likewise, the Mott-Schottky curves were measured at frequency of 500, 1000, 1500 Hz, respectively, with the E_{NHE} standing for E(Ag/AgCl) + 0.197 V.

2.5. Adsorption and photodegradation of Cr(VI)

The adsorption performance of TpPa-SO_3H/Lignin and TpPa-SO_3H was conducted according our previous study (Wang et al., 2021b). Briefly, a series of Cr(VI) solution (5, 25, 50, 75, 100 mg/L) with the initial pH of 6 was prepared in this study. Then, 10 mg TpPa-SO_3H/Lignin and TpPa-SO_3H was added to the Cr(VI) solution, respectively, and the mixtures were incubated 25 ℃ for 120 min. Post-incubation, the Cr(VI) concentrations in the supernatants were quantified using Inductively Coupled Plasma-Mass Spectrometry (ICP-MS). Likewise, the control group was setup without the addition of the TpPa-SO_3H/Lignin or TpPa-SO_3H. Three replicates were performed for each experimental condition.

For the photoreduction assays, experiments were conducted in a photoreaction vessel equipped with two 200 W xenon lamps, providing a light intensity of approximately 300 mW/cm2. Three experimental groups were formed: TpPa-SO_3H/Lignin, TpPa-SO_3H, and a control group. Each group was treated with different pH levels (2.0, 4.0, 6.0, 8.0, 10) for a duration of 210 min. Throughout the reaction period, samples were collected at 30-minute intervals to determine the Cr(III) content using Inductively Coupled Plasma-Mass Spectrometry (ICP-MS).

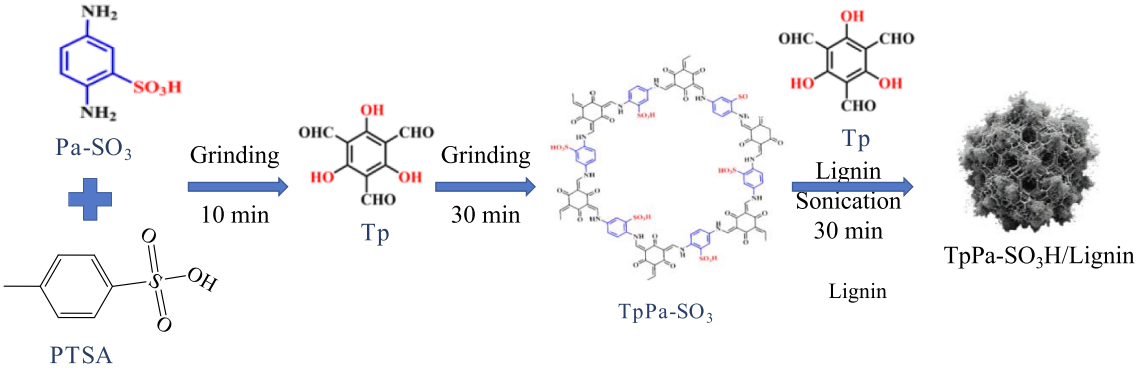

Fig. 1. The synthesis diagram of TaPa-SO_3H/Lignin.

2.6. Determination of the free radicals

According to previous studies, oxygen radicals as the main driving force play an important role in photocatalytic reaction (Xie et al., 2023). Thus, in order to further clarify the mechanisms of bio-composites in the photocatalytic conversion of chromium, the oxygen free radicals in the system was measured via the electron paramagnetic resonance spectroscopy (EPR, Bruker, Germany) in this study. 5,5 dimethyl-1-pyrroline-N-oxide (DMPO) was selected as the radical scavenger. First, samples from different periods were mixed evenly with sodium benzoate, and then free radical capture agents were added to the mixed system for qualitative and quantitative analysis.

3. Results and discussion

3.1. Characteristics of TpPa-SO_3H and TpPa-SO_3H/lignin

The structure characteristics of TpPa-SO_3H and TpPa-SO_3H/lignin were depicted in Fig. 2. Firstly, the FTIR characterization was used to confirm the successful synthesis TpPa-SO_3H and TpPa-SO_3H/lignin. As shown in the Fig. 2 a, the characteristic signals at 1625 cm^{-1}, 1358 cm^{-1}, and 1031 cm^{-1}, corresponding to the C=O, C-N, and O=S=O functional groups, respectively (Zhong et al., 2023). These bands indicate the presence of β-ketoenamine linked frameworks and sulfonic acid groups in both TpPa-SO_3H and TpPa-SO_3H/lignin compounds (Peng et al., 2015). More important, the C=N stretching vibration peaks at 1480 cm^{-1} was observed in the TpPa-SO_3H/lignin, which higher than that the spectra of TpPa-SO_3H, confirming the successful schiff based

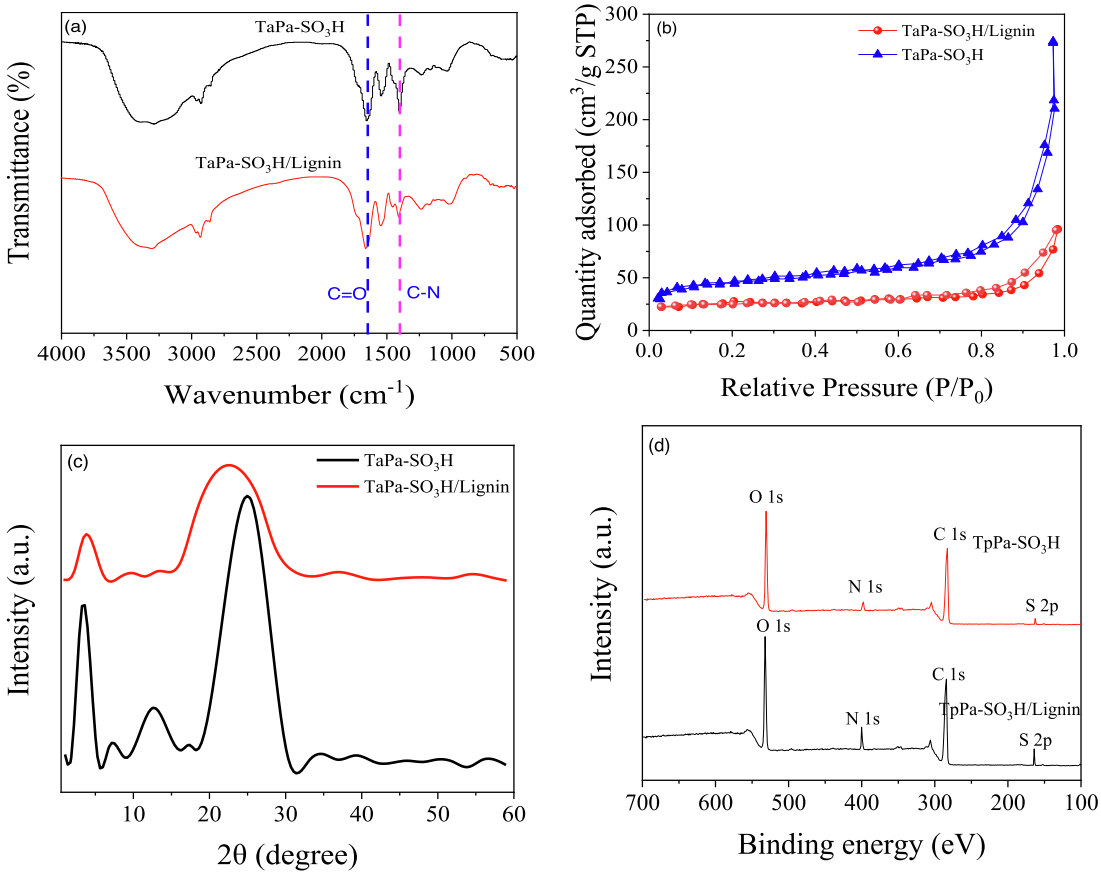

Fig. 2. FTIR spectra (a), N_2-adsorption–desorption isotherm (b), XRD patterns (c) and XPS spectra (d) of TpPa-SO_3H and TpPa-SO_3H/lignin.

reaction between lignin and TpPa-SO_3H (Li et al., 2023b). Likewise, strong peak at the 1265 cm^{-1} and 3437 cm^{-1} were observed in the TpPa-SO_3H/lignin, demonstrating successful integration of the carboxymethyl groups of lignin into the TpPa-SO_3H network, as corroborated by XPS analysis. The XPS results confirmed the observation of C, N, O, S atoms in the TpPa-SO_3H and TpPa-SO_3H/lignin, respectively (Fig. 2d). Likewise, the high resolution XPS spectra of TpPa-SO_3H/lignin and TpPa-SO_3H further validated the chemical states on the surfaces. The three characteristic peaks of N 1 s in TpPa-SO_3H/lignin after peak fitting treatment appeared at 398.5 (C=N), 399.5 (triazine ring), and 399.8 eV (–NH_2) (Fig. S2 d), respectively. The higher intensity of two characteristic peaks obtained by peak fitting treatment of O 1 s appeared at 531.30 (C=O) and 533.38 eV (–COH) (Fig. S1b), respectively. These results further confirming successful incorporation of the powdery TpPa-SO_3H and lignin.

The pore characteristics of TpPa-SO_3H and TpPa-SO_3H/lignin was shown in Fig. 2 b. Results showed that the BET surface area of TpPa-SO_3H/lignin is 75.5 m^2 g^{-1}, which lower than that of the TpPa-SO_3H (120.6 m^2 g^{-1}), aligning with previous research. Zhu et al. (2023) discovered that the specific surface area of lignin-COF films was lower than that of COF, primarily due to the presence of −SO_3H in the channels, obstructing N_2 entry (Zhu et al., 2023). Similarly, Liu et al. (2023) prepared COF/chitosan aerogels and found the specific surface area of COF/chitosan to be significantly lower than that of COF due to reduced crystallinity and the presence of −SO_3 groups in the channels (Liu et al., 2023c). To investigate the evolution of crytallinity in TpPa-SO_3H and TpPa-SO_3H/lignin, XRD analysis was further conducted (Fig. 2c). Results showed that two characteristic peaks were observed in both TpPa-SO_3H and TpPa-SO_3H/Lignin at 5° ((100) planes) and 27° ((001) planes). Likewise, the peak at 5° and 27° were significantly positive correlation with crytallinity and π-π stacking, respectively (Li et al., 2022b; Liu et al., 2023c). In this study, the intensity of TpPa-SO_3H at peak of 5° and 27° was higher than that in TpPa-SO_3H/lignin, indicating that TpPa-SO_3H has higher value of crystallinity and π-π stacking. Meanwhile, the peak at 5° and 27° in the TpPa-SO_3H/lignin showed a wider peak shape, indicating that TpPa-SO_3H/lignin has irregular

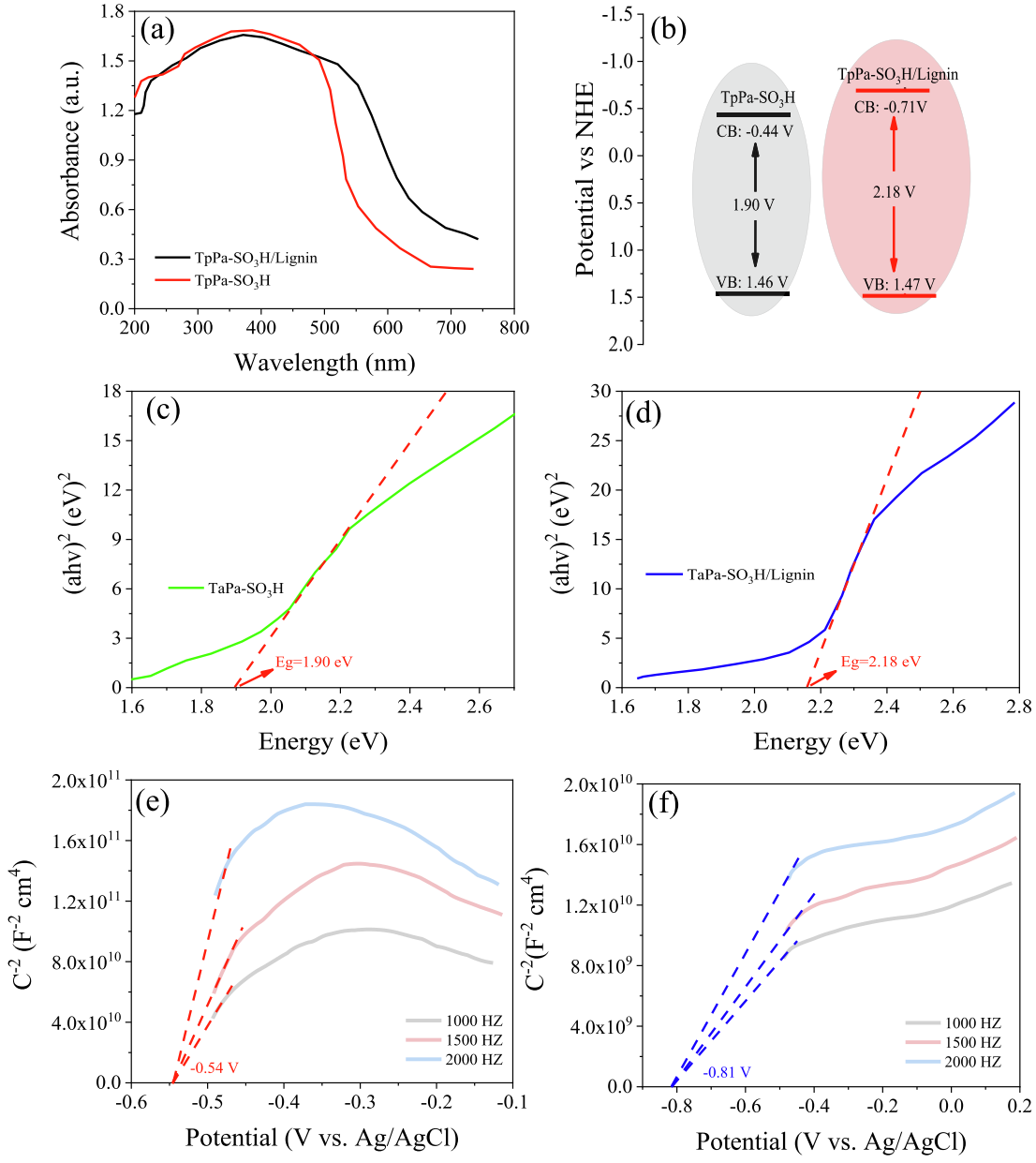

Fig. 3. UV–vis absorption spectra (a), the electronic band structure (b), the plot of $(ahv)^2$ versus photo energy (hv) (c and d)and Mott-Schottky plot of TpPa-SO_3H (e) and TpPa-SO_3H/Lignin (f).

stacking, which may be the main reason for the lower crystallinity of TpPa-SO_3H/lignin.

3.2. The electrochemical properties of TpPa-SO_3H and TpPa-SO_3H/lignin

The electrochemical properties of TpPa-SO_3H and TpPa-SO_3H/lignin was shown in Fig. 3 a. A wide visible light adsorption rang was observed in both TpPa-SO_3H and TpPa-SO_3H/lignin, indicating that both materials can absorb visible light to generate photoelectrons for photocatalytic reactions. Compared to the TpPa-SO_3H, a higher value of visible range was observed in TpPa-SO_3H/lignin, which was attribution to the introduction of lignin into TpPa-SO_3H. According to the previous studies, the visible light absorption range of COFs is usually related to the strength of its internal electric field, and its electric field intensity is positively correlated with the type and number of electron-absorbing groups (e.g., −Cl, −SO_3H, –COOH and –NO_2 groups) (Wang et al., 2024b; Deng et al., 2024). For instances, Zhong et al. (2023) confirmed that the electron-withdrawing ability of –COOH and –OH groups was higher than that of −Cl, –NO_2 groups. There are abundant –COOH, –OH and quinone groups in the lignin structure, which may be the main reason why TpPa-SO_3H/lignin has a wide visible light range.

Furthermore, in order to further investigate the electrochemical characteristics of TpPa-SO_3H and TpPa-SO_3H/lignin, the Mott-Schottky curves was conducted in this study. A positive slope of the Mott-schottky curve was observed in this study, indicating that TpPa-SO_3H and TpPa-SO_3H/lignin are the typical n-type semiconductors (Li et al., 2018; Zhong et al., 2023; Wang et al., 2023b, 2023a). Moreover, the flat band potential of TpPa-SO_3H and TpPa-SO_3H/lignin were approximately −0.54 V and −0.81 V (vs Ag/AgCl) (Fig. 3 e and f). Similarly, the conduction band, valence band and band gap of TpPa-SO_3H and TpPa-SO_3H/lignin can be calculated based on the flat band potential and Kubelka-Munk function (Li et al., 2023a; Wang et al., 2023c; Zhang et al., 2021). Generally, the conduction band is negatively correlated with the photocatalytic performance, while the valence band and band gap values are positively correlated with the photocatalytic performance of the semiconductors. In this study, the conduction bands of TpPa-SO_3H and TpPa-SO_3H/lignin are −0.44 V and −0.71 V respectively, while the band gaps of TpPa-SO_3H and TpPa-SO_3H/lignin are 1.90 V and 2.18 V respectively (Fig. 3 c and d). Therefore, the valence bands of TpPa-SO_3H and TpPa-SO_3H/lignin are 1.46 V and 1.47 V respectively (Fig. 3 b). These results indicated that TpPa-SO_3H/lignin has a higher value of the photocatalytic performance.

3.3. The adsorption-photocatalytic properties of TpPa-SO_3H and TpPa-SO_3H/lignin

First, the adsorption properties of TpPa-SO_3H and TpPa-SO_3H/lignin for hexavalent chromium were explored under dark conditions and different hexavalent chromium concentration, respectively. A decreased trend of the removal efficiency of TpPa-SO_3H for Cr(VI) was observed with the increase of initial Cr(VI) concentration (Fig. 4a). In detail, TpPa-SO_3H showed the maximum adsorption capacity in the low chromium concentration range (5 ~ 25 mg/L), which was consistent with previous study (Zhong et al., 2023; Li et al., 2024). When the initial ion concentration is low, the active functional groups can fully combine with the ions to achieve higher removal efficiency. Otherwise, the ion concentration is in excess, resulting in a decrease in removal efficiency. Compared to the TpPa-SO_3H, a higher value of removal was observed in TpPa-SO_3H/lignin under the range of 5 ~ 100 mg/L (Fig. 4b). Within the initial concentration range of 5 ~ 50 mg/L, the removal efficiency of TpPa-SO_3H/lignin is stable at 100 %. At the same time, when the initial concentration increases to 100 mg/L, the removal efficiency of Cr(VI) by TpPa-SO_3H/lignin reaches 92 %. This finding can be described by the presence of various functional groups (e.g., phenolic hydroxyl, carboxyl, and quinone groups) in the lignin, thereby improving the adsorption performance of TpPa-SO_3H/lignin (Xie et al., 2023; Wang et al., 2021a).

Furthermore, the photocatalytic reduction performance of Cr(VI) by the TpPa-SO_3H and TpPa-SO_3H/lignin were conducted under dark and light conditions (Fig. 5a). Likewise, in order to better evaluate the effect of TpPa-SO_3H and TpPa-SO_3H/lignin on the photocatalytic reduction of Cr(VI), a blank experiment without adding photocatalyst was also set up. The results of dark and blank control experiments showed that no obvious photocatalytic reduction process occurred. In the light conditions, results showed that the photocatalytic reduction efficiency of Cr (VI) by TpPa-SO_3H (26.5 %) was significantly lower than that of TpPa-SO_3H/lignin (72.5 %) during the 210 min reaction process. Moreover, a higher K values were found in TpPa-SO_3H/lignin (0.00534 min^{-1}) compared to the TpPa-SO_3H (0.00312 min^{-1}), further indicating that the higher photocatalytic efficiency of TpPa-SO_3H/lignin (Fig. 4c).

Moreover, the effect of solution pH on the photocatalytic of Cr(VI) by TpPa-SO_3H/lignin was investigated in this study. Results showed that a significant different of photocatalytic efficiency of TpPa-SO_3H/lignin was observed in the different initial pH value (Fig. 5 b). The photocatalytic efficiency of TpPa-SO_3H/lignin showed a decreased trend with the increase of pH value, and a maximum photocatalytic efficiency was determined at the pH value of 2 (98.56 %). While, the photocatalytic efficiency of Cr(VI) by TpPa-SO_3H/lignin at the pH value of 10 was the 30.41 %. Moreover, the K value of the pseudo-first order dynamic models follow the order of pH 2 (0.01333 min^{-1}) > pH 4 (0.01005 min^{-1}) > pH 6 (0.00496 min^{-1}) = pH 8 (0.00496 min^{-1}) > pH 10 (0.00216 min^{-1}) (Fig. 4d). The K value of pH 2 was 6.17 times of pH 10, which is responsible for the photocatalyst efficiency of Cr(VI) by TpPa-SO_3H/lignin results. Generally, Cr(VI) mainly exists in the form of $Cr_2O_7^{2-}$, $HCrO_4^-$ and CrO_4^{2-} under acidic conditions and alkaline

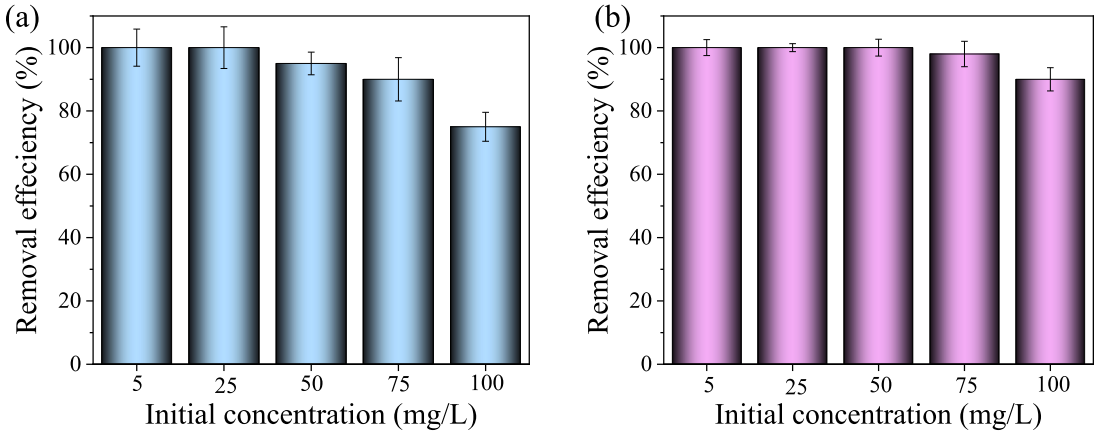

Fig. 4. The removal efficiency of Cr(VI) by TpPa-SO_3H (a) and TpPa-SO_3H/lignin (b) under the different initial Cr(VI) concentration.

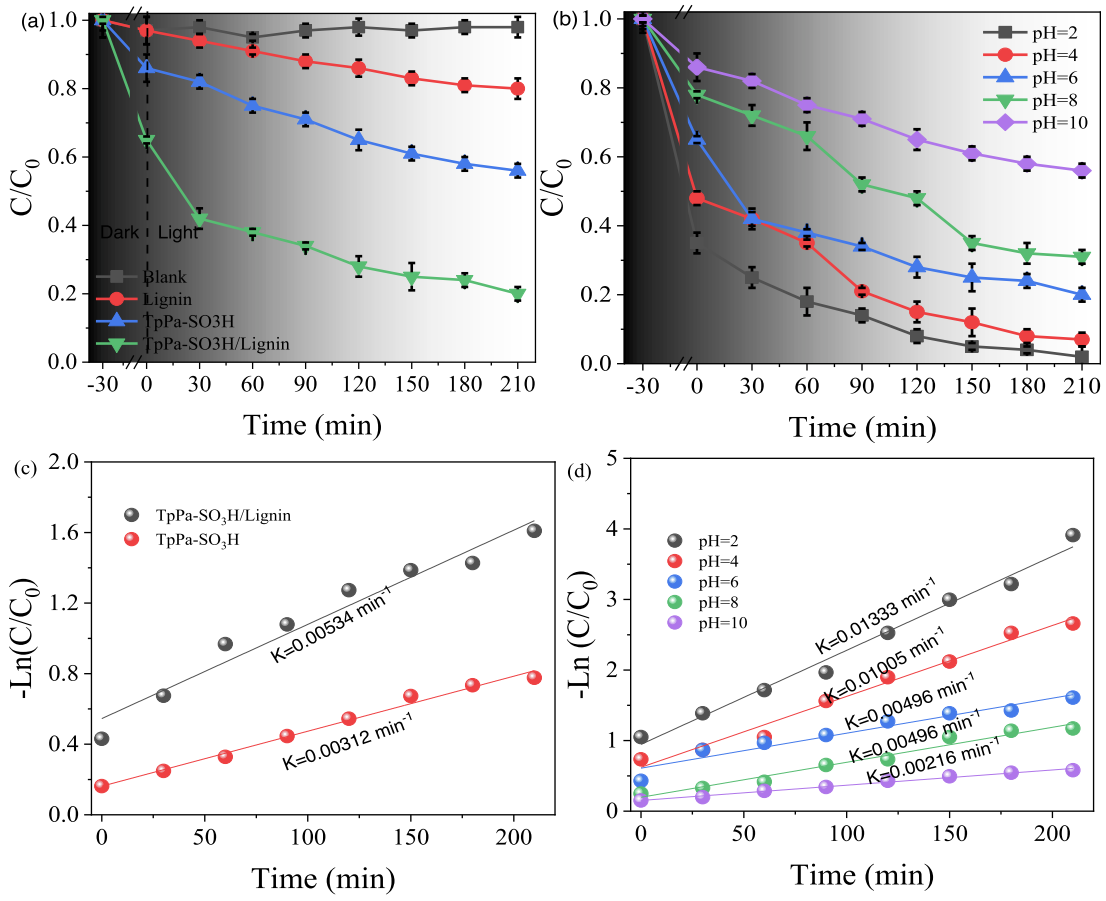

Fig. 5. Photocatalytic reduction of Cr(VI) under the different materials (a) and different initial pH value (b), and the corresponding pseudo-first-order rate constant (k) of Cr(VI) photoreduction.

conditions, respectively (Yang et al., 2021; Sun et al., 2023). In the redox process, the redox potential of $Cr_2O_7^{2-}$ and $HCrO_4^-$ under acidic conditions is significantly higher than that of CrO_4^{2-} under alkaline conditions, so $Cr_2O_7^{2-}$ and $HCrO_4^-$ are more easily photocatalytically reduced under acidic conditions. In addition, the forms of $Cr_2O_7^{2-}$, $HCrO_4^-$ and CrO_4^{2-} have different solubilities under different pH conditions. In particular, CrO_4^{2-} can easily react with –OH under alkaline conditions to form Cr $(OH)_3$ precipitates (Yang et al., 2021), thereby reducing the photocatalytic efficiency.

Furthermore, in order to evaluate the reusability of the TpPa-SO_3H/Lignin, seven cycles of photocatalytic reduction studies were conducted in this study. As shown in Fig. 6 a, after seven times of continuous usage, the photocatalytic Cr(VI) reduction performance of TpPa-SO_3H/Lignin was still excellent, and the Cr(VI) removal rate reached 90.25 %, indicated that the TpPa-SO_3H/Lignin composite was stable and recyclable during test. Likewise, the XRD patterns of TpPa-SO_3H/Lignin before and after seven cycles test was shown in Fig. 5 b. Results showed that TpPa-SO_3H/Lignin still ensured complete peaks, and the intensity of the peaks had not diminished after photocatalytic cycles. This result indicated that TpPa-SO_3H/Lignin had a stronger structure stability.

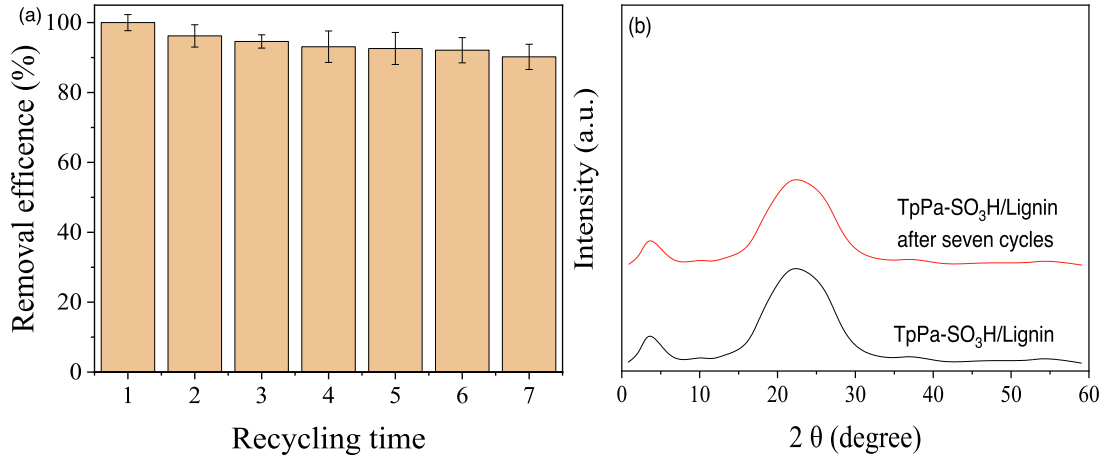

Fig. 6. The reusability of the TpPa-SO_3H/Lignin composites (a) and the XRD patterns of TpPa-SO_3H/Lignin before and after seven cycles (b).

3.4. Possible mechanism of photocatalytic reduction of Cr(VI) by TpPa-SO_3H/lignin

Previous studies have shown that photocatalytic efficiency is significantly related to the separation transfer rate of photogenerated electrons and the generation rate of oxygen free radicals of photocatalytic materials (Chen et al., 2023; Sun et al., 2023). Thus, photoluminescence (PL) emission spectroscopy, electron spin resonance (ESR) and electrochemical impedance spectroscopy (EIS) were used to elucidate the potential mechanism of photocatalytic conversion of Cr(VI) by TpPa-SO_3H/lignin. Two intense emission peaks were observed at 470 nm and 495 nm for TpPa-SO_3H and TpPa-SO_3H/lignin, respectively, and the intensity of these peaks in TpPa-SO_3H/lignin was higher than that of TpPa-SO_3H (Fig. 7a). According to the previous studies, the peaks of 470 nm and 495 nm were corresponding to the the recombination rate of photogenerated electrons (e^-) and holes (h^+) (Zheng et al., 2021). Likewise, the intensity of these peaks was negative related to the recombination rate of photogenerated electrons (e^-) and holes (h^+). Thus, the recombination rate of photogenerated electrons (e^-) and holes (h^+) of TpPa-SO_3H/lignin was lower than that of TpPa-SO_3H. Moreover, the recombination rate of photogenerated e^- and h^+ was negative related to the efficiency of charge separation and transfer (Zhong et al., 2023). Consequently, the charge separation and transfer efficiency in the TpPa-SO_3H/lignin composite is superior to that in TpPa-SO_3H. These findings imply that the introduction of a heterogeneous structure significantly amplifies the material's photoreactivity, which is consistent with the Electrochemical Impedance Spectroscopy (EIS) results (Fig. 7b). The EIS results showed that all tested samples displayed arc-shaped semicircles in their EIS profiles. Notably, the arc radius for the TpPa-SO_3H/lignin composite is markedly smaller than that of TpPa-SO_3H, indicating a lower resistance in the composite. Hence, it can be inferred that the efficient photoelectron transfer between the constituents in the TpPa-SO_3H/lignin composite facilitates electron-hole separation, thereby elevating the photocatalytic reduction efficiency for Cr(VI) (Zhong et al., 2023). Moreover, the electron spin resonance (ESR) was used to determine the free radicals of TpPa-SO_3H and TpPa-SO_3H/lignin, respectively. Results showed that the signals of ▪O_2^- and ▪OH were determined in the photocatalyst process of Cr (VI) by TpPa-SO_3H and TpPa-SO_3H/lignin (Fig. S1). Likewise, the signal intensity of TpPa-SO_3H/lignin is significantly higher than that of TpPa-SO_3H. These results indicated that active free radicals generated during the photocatalyst process (Xie et al., 2023). In order to further investigate the the impact of different active free radicals on photocatalytic efficiency, we selected isopropyl alcohol (free radical scavenger of OH), p-benzoquinone (e-inhibitor), KIO_3 ($\cdot O_2^-$inhibitor), EDTA-2Na (hole h^+ trapping agent) was used to conduct experiments on photocatalytic efficiency (Fig. 7c). The results showed that after adding KIO_3 and p-benzoquinone, the photocatalytic efficiency of TpPa-SO_3H/lignin towards Cr(VI) dropped from 98.56 % to 40.25 % and 38.29 % respectively. After adding isopropyl alcohol, the photocatalytic efficiency of TpPa-SO_3H/lignin for Cr(VI) has no significant change. This result shows that e- and $\cdot O_2^-$ are generated and played an important role during the photocatalytic reaction, while the contribution of ·OH to Cr(VI) photoreduction is negligible.

Based on above results, the possible mechanism of photocatalytic reduction of Cr(VI) by TpPa-SO_3H/lignin was given in Fig. 8. The redox of Cr(VI) is significantly associated with reactive oxygen species (ROS). Generally, the generation of ROS primarily occurs through the reduction of dissolved oxygen in water and the inherent pathways of the photocatalytic material (Sun et al., 2023). Among these, the reduction of dissolved oxygen is significantly related to the standard potential of $O_2/\cdot O_2^-$ (−0.33 V vs. NHE) and the photocatalytic material. In this study, the negative conduction band of TpPa-SO_3H/lignin (−0.91 V) was much lower than that of the standard potential of $O_2/\cdot O_2^-$ (−0.33 V vs. NHE), thus enhancing the conversion of dissolved oxygen in water to $\cdot O_2^-$ under the action of photogenerated electrons formed from the TpPa-SO_3H/lignin, thereby increasing the concentration of $\cdot O_2^-$. The efficiency of the spontaneous generation of $\cdot O_2^-$ by photocatalytic materials is related to the structure of the material. Previous research has indicated a negative correlation between the structure of photocatalytic materials, specifically the electrical resistance, and the efficiency of charge separation and transfer. In this study, TpPa-SO_3H/lignin exhibits higher electrical resistance, enhancing its responsiveness to light and thereby boosting the effective transfer of photoelectrons. This structural characteristic leads to the accumulation of photogenerated electrons on the TpPa-SO_3H/lignin conduction band, enhancing the generation efficiency of ROS, and consequently improving the reduction rate of Cr(VI). Notably, the advantage of this photocatalytic reaction is its effective utilization of solar energy as a light source, thereby achieving both environmental friendliness and cost-effectiveness. The unique structure and properties of TpPa-SO_3H/lignin not only reduce energy consumption but also enhance the efficiency of the photocatalytic process. Furthermore, the development and application of such materials are of significant importance for environmental purification and the advancement of sustainable energy technologies. Through these studies, we can gain a deeper understanding and control of the photocatalytic process, thus providing more effective solutions for environmental protection and energy conversion.

4. Environmental implication

Utilization of waste to prepare efficient photosensitive materials for rapid and efficient removal of Cr(VI) is extremely vital for waste resource utilization and environmental protection. The newly developed bio-composites proves highly effective in Cr(VI) removal. The introduction of lignin enhances visible light response, charge separation, and photogenerated carriers, significantly improving the photocatalytic efficiency of Cr(VI) removal. The observed 98.56 % efficiency under acidic conditions further underscores its versatility. This research provides a sustainable and efficient approach to mitigating Cr(VI) pollution, with broader implications for employing lignocellulose-derived materials, in

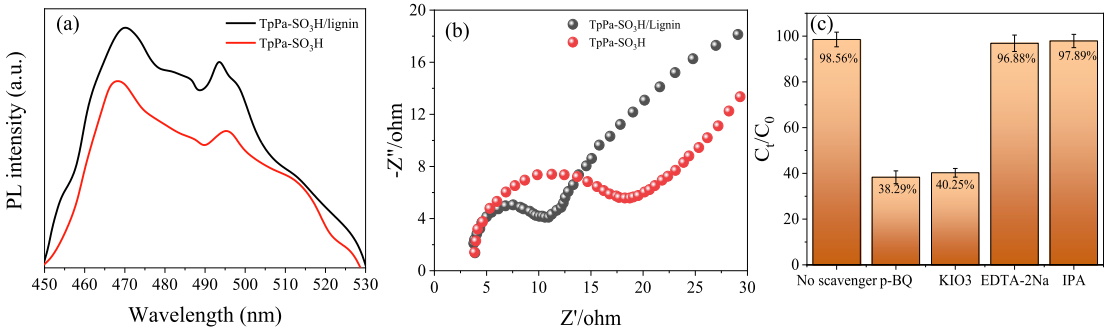

Fig. 7. PL spectra at the 385 nm (a) and EIS plots (b) of the as TpPa-SO_3H and TpPa-SO_3H/Lignin; The effect of different scavengers on the photocatalytic reduction of Cr (VI) (c).

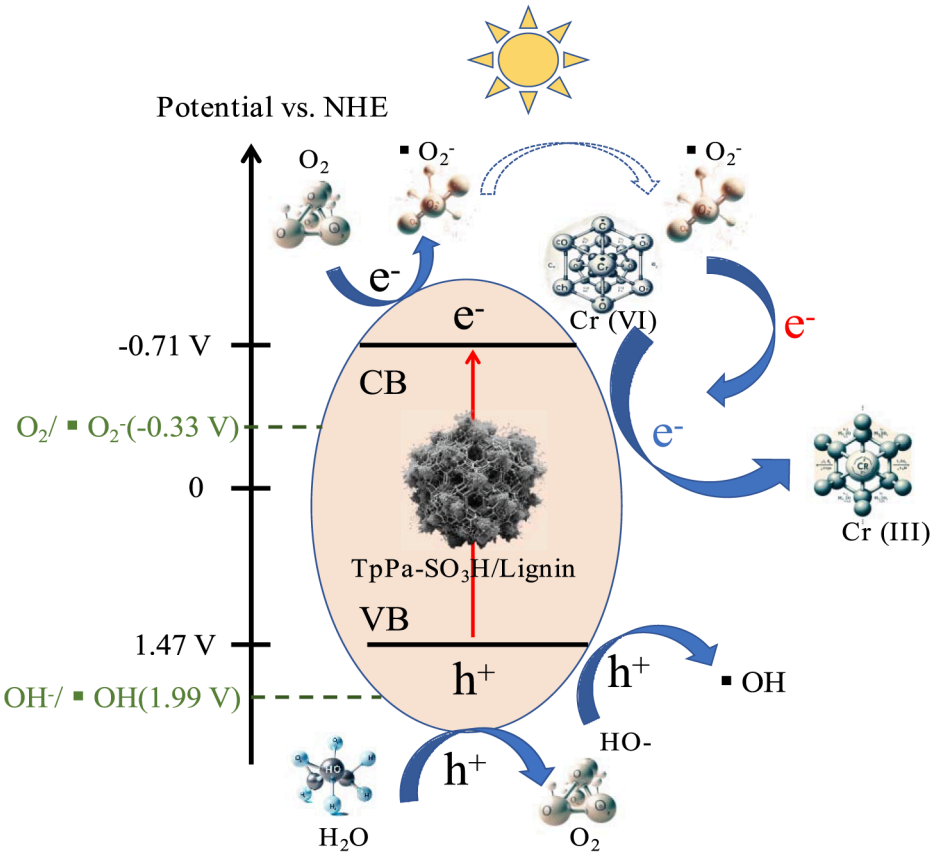

Fig. 8. The potential possible mechanism of photocatalytic reduction of Cr (VI) by TpPa-SO_3H/lignin.

diverse environmental applications, advancing eco-friendly solutions for heavy metal contamination.

5. Conclusion

In this study, a novel a novel material integrating agricultural waste (lignin) with covalent organic frameworks was synthesized using a dual cross-linking approach. The novel composite, TpPa-SO_3H/lignin, was thoroughly characterized to assess its physical and chemical properties. A key finding of this research is the enhanced adsorption-photocatalytic reduction efficiency of hexavalent chromium (Cr(VI)) due to the effective incorporation of lignin into the covalent organic framework. The material maintained an impressive 100 % adsorption removal efficiency for Cr(VI) across a concentration range of 5–75 mg/L. Moreover, TpPa-SO_3H/lignin exhibited superior photogenerated electron separation and transfer capabilities, leading to optimal photocatalytic performance. Under optimal conditions, the photocatalytic reduction of Cr(VI) achieved a remarkable removal rate of 98.56 %, with a reaction rate constant (k) of 0.01333 min^{-1}. The reduction mechanism of Cr(VI) by TpPa-SO_3H/lignin was elucidated through Electron Spin Resonance (ESR) testing, radical trapping experiments, and energy band theory analysis. In conclusion, TpPa-SO_3H/lignin emerges as a highly effective and innovative material for the removal of Cr(VI), demonstrating significant potential for environmental remediation applications.

CRediT authorship contribution statement

Huiying Hu: Investigation, Data curation. **Kaijian Bi:** Resources, Methodology. **Haizhong Yu:** Validation, Software, Conceptualization. **Pengjiao Tian:** Writing – original draft, Visualization. **Xiqing Wang:** Writing – review & editing, Supervision.

Acknowledgement

This study support by the International Science and Technology Cooperation Project of Hubei Province (2023EHA051), Natural Science Foundation of Hubei Province Cultivation Program (2022CFD096), Xiangyang City Science and Technology Bureau Project (2022ABA006208) and Ministry of Education of the People's Republic of China Research, China (202201618).

Appendix A. Supplementary material

Supplementary data to this article can be found online at https://doi.org/10.1016/j.arabjc.2024.105980.

References

Cao, Z.L., Wang, M.Y., Gao, H.M., Li, L.Y., Ren, S.J., 2022. Porous organic polymers via diels-alder reaction for the removal of Cr(VI) from aqueous solutions. ACS Macro Lett. 11 (4), 447–451.

Chen, P., Di, S.Y., Xie, W.X., Li, Z.H., Zhu, S.K., 2023. One-step synthesis of triazine-based covalent organic frameworks at room temperature for efficient photodegradation of bisphenol A under visible light irradiation. Front. Mater. Sci. 17 (4), 230661.

Chen, S., Xia, Y., Zhang, B., Chen, H., Chen, G., Tang, S., 2021. Disassembly of lignocellulose into cellulose, hemicellulose, and lignin for preparation of porous carbon materials with enhanced performances. J. Hazard. Mater. 408, 124956.

Côté, A.P., Benin, A.I., Ockwig, N.W., O'Keeffe, M., Matzger, A.J., Yaghi, O.M., 2005. Porous, crystalline, covalent organic frameworks. Science 310 (5751), 1166–1170. https://doi.org/10.1055/s- 2006-931943.

Deng, M., Guo, J.Y., Ma, X., Fu, Y.J., Du, H., Hao, D.R., Wang, Q., 2023. Enhanced photocatalytic Cr(VI) reduction performance by novel PDI/COFs composite. Sep. Purif. Technol. 326, 124786.

Deng, H., Hui, X.Y., Zhang, C., Zhou, Q., Li, Q., Du, H., Hao, D.R., Yang, G.X., Wang, Q., 2024. MXene-derived quantum dots based photocatalysts: Synthesis, application, prospects, and challenges. Chinese Chem. Let. 35 (6), 109078.

Fan, C., Qian, J., Yang, Y., Sun, H., Song, J., Fan, Y., 2021. Green ceramsite production via calcination of chromium contaminated soil and the toxic Cr(VI) immobilization mechanisms. J. Clean. Prod. 315, 128204.
Izzudin, N.M., Jalil, A.A., Aziz, F.F.A., Azami, M.S., Ali, M.W., Hassan, N.S., Rahman, A. F.A., Fauzi, A.A., Vo, D.V.N., 2021. Simultaneous remediation of hexavalent chromium and organic pollutants in wastewater using period 4 transition metal oxide-based photocatalysts: a review. Environ. Chem. Lett. 19 (6), 4489–4517.
Jiang, B., Gong, Y., Gao, J., Sun, T., Liu, Y., Oturan, N., Oturan, M.A., 2019. The reduction of Cr(VI) to Cr(III) mediated by environmentally relevant carboxylic acids: state-of-the-art and perspectives. J. Hazard. Mater. 365, 205–226.
Jiang, Y., Yang, F., Dai, M., Ali, I., Shen, X., Hou, X., Alhewairini, S.S., Peng, C., Naz, I., 2022. Application of microbial immobilization technology for remediation of Cr(VI) contamination: a review. Chemosphere 286, 131721.
Li, Q., Ge, C.B., Ma, J.G., Gu, S.J., Yang, H., Xiong, Y., Zhou, H., Du, H., Zhu, H.Y., Wang, Q., 2024. MXenes-based adsorbents for environmental remediation. Sep. Purif. Technol. 342, 126982.
Li, C., Liu, J., Li, H., Wu, K., Wang, J., Yang, Q., 2022a. Covalent organic frameworks with high quantum efficiency in sacrificial photocatalytic hydrogen evolution. Nat. Commun. 13, 2357.
Li, L., Tian, F., Qiu, L., Wu, F., Yang, W., Yu, Y., 2023a. Recent progress on ruthenium-based electrocatalysts towards the hydrogen evolution reaction. Catalysts 13 (12), 1497.
Li, W., Wang, Q., Cui, F., Jiang, G., 2022b. Covalent organic framework with sulfonic acid functional groups for visible light-driven CO2 reduction. RSC Adv. 12, 17984–17989.
Li, Q., Xia, Y., Yang, C., Lv, K., Lei, M., Li, M., 2018. Building a direct Z-scheme heterojunction photocatalyst by ZnIn2S4 nanosheets and TiO2 hollowspheres for highly-efficient artificial photosynthesis. Chem. Eng. J. 349, 287–296.
Li, Y., Yang, L., He, H., Sun, L., Wang, H., Fang, X., Zhao, Y., Zheng, D., Qi, Y., Li, Z., Deng, W., 2022c. In situ photodeposition of platinum clusters on a covalent organic framework for photocatalytic hydrogen production. Nat. Commun. 13, 1355.
Li, N., Yao, B., Xiong, X.L., Zhu, P.F., Xi, L.F., 2023b. Recent advanced in adsorption removal and photocatalytic reduction of Cr (VI) by porous organic polymers (POPs). Eur. Polym. J. 200, 112530.
Liu, J., Sun, S., Zhang, H., Kong, Q., Li, Q., Yao, X., 2023a. Remediation materials for the immobilization of hexavalent chromium in contaminated soil: preparation, applications, and mechanisms. Environ. Res. 237, 116918.
Liu, L.C., Sun, P., Chen, Y.Y., Li, X.C., Zheng, X.L., 2023b. Distinct chromium removal mechanisms by iron-modified biochar under varying pH: Role of iron and chromium speciation. Chemosphere 331, 138796.
Liu, K., Yang, J., Liu, J., Shuai, Q., Yamauchi, Y., Han, M., Huang, L., 2023c. Robust self-floating covalent organic framework/chitosan aerogels for the efficient removal of sulfamerazine. Chem. Eng. J. 472, 144966.
Ma, X., Du, H., Tan, M., Qian, J.Y., Deng, M., Hao, D.R., Wang, Q., Zhu, H.Y., 2024. Photocatalytic fuel cell with cathodic P-BiVO4/CQDs and anodic WO3 for efficient Cr(VI) reduction and stable electricity generation. Sep. Purif. Technol. 339, 126644.
Malaviya, P., Singh, A., 2011. Physicochemical Technologies for Remediation of Chromium-Containing Waters and Wastewaters. Crit. Rev. Environ. Sci. Technol. 41 (12), 1111–1172.
Ministry of Environmental Protection and the Ministry of Land and Resources, 2014. http://www.gov.cn/xinwen/2014-04/17/content_2661765.htm.
Nakkeeran, E., Patra, C., Shahnaz, T., Rangabhashiyam, S., Selvaraju, N., 2018. Continuous biosorption assessment for the removal of hexavalent chromium from aqueous solutions using Strychnos nux vomica fruit shell. Bioresour. Technol. Rep. 3, 256–260.
Peng, L., Chang, S., Liu, Z., Fu, Y., Ma, R., Lu, X., Zhang, F., Zhu, W., Kong, L., Fan, M., 2021. Visible-light-driven photocatalytic CO2 reduction over ketoenamine-based covalent organic frameworks: role of the host functional groups. Catal. Sci. Technol. 11 (5), 1717–1724.
Peng, Y., Hu, Z., Gao, Y., Yuan, D., Kang, Z., Qian, Y., Yan, N., Zhao, D., 2015. Synthesis of a sulfonated two-dimensional covalent organic framework as an efficient solid acid catalyst for biobased chemical conversion. ChemSusChem 8 (19), 3208–3212.
Prasad, S., Yadav, K.K., Kumar, S., Gupta, N., Cabral-Pinto, M.M.S., Rezania, S., Radwan, N., Alam, J., 2021. Chromium contamination and effect on environmental health and its remediation: a sustainable approaches. J. Environ. Manage. 285, 112174.
Shan, H., Cai, D., Zhang, X., Zhu, Q., Qin, P., Baeyens, J., 2023. Donor-acceptor type two-dimensional porphyrin-based covalent organic framework for visible-light-driven heterogeneous photocatalysis. Chem. Eng. J. 432, 134288.
Shen, X., Dai, M., Yang, J., Sun, L., Tan, X., Peng, C., Ali, I., Naz, I., 2022. A critical review on the phytoremediation of heavy metals from environment: performance and challenges. Chemosphere 291, 132979.
Sheng, J.L., Dong, H., Meng, X.B., Tang, H.L., Yao, Y.H., Liu, D.Q., Bai, L.L., Zhang, F.M., Wei, J.Z., Sun, X.J., 2019. Effect of different functional groups on photocatalytic hydrogen evolution in covalent-organic frameworks. ChemCatChem 11, 2313–2319.
Su, H., Fang, Z., Eric, P., Fang, J., 2016. Stabilization of nanoscale zero-valent iron with biochar for enhanced transport and in-situ remediation of hexavalent chromium in soil. Environ. Pollut. 214, 94–100. https://doi.org/10.1016/j.envpol.2016.03.072.
Sun, L., Dong, S., Chen, S., Chen, H., Luan, M., Huang, T., 2023. Efficient reduction of hexavalent chromium by nubbly mesoporous NH2-MIL-125(Ti)/SnS2 Z-scheme heterostructures with enhanced visible photocatalytic activity. J. Environ. Chem. Eng. 11, 110192.
Wang, Y., Bao, S., Liu, X., Qiu, L., Sheng, J., Yang, W., Yu, Y., 2023b. Regulating the peroxymonosulfate activation on N doped δ-MnO2 nanosheets for tetracycline degradation: N species as the degradation pathways switcher to convert radical to nonradical. Chem. Eng. J. 477, 147050.
Wang, X., Lyu, T., Dong, R., Liu, H., Wu, S., 2021b. Dynamic evolution of humic acids during anaerobic digestion: exploring an effective auxiliary agent for heavy metal remediation. Bioresour. Technol. 320, 124331.
Wang, Q., Ma, W.G., Qian, J.Y., Li, N.Y., Zhang, C., Deng, M., Du, H., 2024a. S-scheme towards interfacial charge transfer between POMs and MOFs for efficient visible-light photocatalytic Cr(VI) reduction. Environ. Pollut. 347, 123707.
Wang, X., Muhmood, A., Lyu, T., Dong, R., Liu, H., Wu, S., 2021a. Mechanisms of genuine humic acid evolution and its dynamic interaction with methane production in anaerobic digestion processes. Chem. Eng. J. 408, 127322.
Wang, Y., Qiu, L., Bao, S., Tian, F., He, L., Yang, W., Liu, Y., Yu, Y., 2023a. In situ construction of MnIn2S4/Ti3C2Tx MXene Schottky junction composites for efficient photoreduction and recovery of U(VI). Chem. Eng. J. 468, 143768.
Wang, Y., Qiu, L., Bao, S., Tian, F., Sheng, J., Yang, W., Yu, Y., 2023c. Visible-light enhanced peroxymonosulfate activation on Co3O4/MnO2 for the degradation of tetracycline: cooperation of radical and non-radical mechanisms. Sep. Purif. Technol. 316, 123779.
Wang, Q., Zhou, H., Qian, J.Y., Xue, B., Du, H., Hao, D.R., Ji, Y., Li, Q., 2024b. b. $Ti_{3\ C}2$ -assisted construction of Z-scheme MIL-88A(Fe)/T_i3_C2/RF heterojunction: multifunctional photocatalysis-in-situ-self-Fenton catalyst. J. Mat. Sci. Technol. 190, 67–75.
Xie, M., Ren, D., Muhmood, A., Tian, P., Su, Y., Wang, X., 2023. Revealing the effect of humic substance compounds on the aged characteristics and release compounds profiles from photodegradation of polyethylene microplastics. Arab. J. Chem. 16, 105157.
Yang, J., Ghosh, S., Roeser, J., Acharjya, A., Penschke, C., Tsutsui, Y., Rabeah, J., Wang, T., Djoko Tameu, S.Y., Ye, M.Y., Gruneberg, J., Li, S., Li, C., Schomacker, R., Van De Krol, R., Seki, S., Saalfrank, P., Thomas, A., 2022b. Constitutional isomerism of the linkages in donor-acceptor covalent organic frameworks and its impact on photocatalysis. Nat. Commun. 13, 6317.
Yang, Y., Kang, J., Li, Y., Liang, J., Liang, J., Jiang, L., Chen, D., He, J., Chen, Y., Wang, J., 2022a. Enhanced photocatalytic hydrogen peroxide production activity of imine-linked covalent organic frameworks via modification with functional groups. New J. Chem. 46, 21605–21614.
Yang, W., Yang, Z., Shao, L., Li, S., Liu, Y., Xia, X., 2021. Photocatalytic reduction of Cr (VI) over cinder-based nanoneedle in presence of tartaric acid: synergistic performance and mechanism. J. Environ. Sci. 107, 194–204. https://doi.org/10.1016/j. jes.2021.02.006.
Yin, L., Zhao, Y., Xing, Y., Tan, H., Lang, Z., Ho, W., Wang, Y., Li, Y., 2021. Structure-Property relationship in β-keto-enamine-based covalent organic frameworks for highly efficient photocatalytic hydrogen production. Chem. Eng. J. 419, 129984.
Zeng, Y., Zou, R., Zhao, Y., 2016. Covalent organic frameworks for CO2 capture. Adv. Mater. 28, 2855–2873.
Zhang, J., Cao, Y., Liu, W., Cao, T., Qian, J., Wang, J., Yao, X., Iqbal, A., Qin, W., 2022. Structural engineering of covalent organic frameworks comprising two electron acceptors improves photocatalytic performance. ChemSusChem 15, e202101510.
Zhang, X., Tian, F., Qiu, L., Gao, M., Yang, W., Liu, Y., Yu, Y., 2021. Z-scheme Mo2C/MoS2/In2S3 dual-heterojunctions for the photocatalytic reduction of Cr(VI). J. Mater. Chem. a. 9, 10297–10303.
Zheng, X., Li, Y., Yang, J., Cui, S., 2021. Z-Scheme heterojunction Ag/NH2-MIL-125(Ti)/CdS with enhanced photocatalytic activity for ketoprofen degradation: mechanism and intermediates. Chem. Eng. J. 422, 130105 https://doi.org/10.1016/j.cej.2021.130105.
Zhong, X., Ling, Q., Kuang, P., Hu, B., 2023. The role of functional-group-tuning in adsorption-photoreduction of U(VI) onto B-ketoenamine covalent organic frameworks photosystem. Chem. Eng. J. 467, 143415.
Zhu, L., Ye, P., Zhang, L., Ren, Y., Liu, J., Lei, J., Wang, L., 2023. Bioinspired heterogeneous construction of lignocellulose-reinforced COF membranes for efficient proton conduction. Nano Micro Small 2304575.